Electronic Supplementary Information

Design Strategy of Encapsulated Nanoplates and Nanorods (ID-CoMo): Enhanced High Catalytic Activity and Sustainability for Overall & Solar Cell Water Splitting

Muthukumaran Sangamithirai, Murugan Vijayarangan, Arunagiri Gayathri, Murugan Muthamildevi and Jayaraman Jayabharathi*

Department of Chemistry, Material Science Lab, Annamalai University, Annamalai Nagar, Tamil Nadu-608 002, India

**Email id: jtchalam2005@yahoo.co.in*

Contents

SI-I: Experimental Section

Chemicals

Cobalt (II) sulfate ($CoSO_4.7H_2O$) purchased in Sigma Aldrich, Ammonium molybdate ($(NH_4)_6Mo_7O_{24}$) purchased in Ottokemi, com and potassium hydroxide (KOH) purchased in EMPLURA. All reagents are analytically pure without further purification. Deionized water was used throughout the experiment.

Characterization of an electrocatalyst

The morphologies and chemical compositions of catalyst samples were determined by scanning electron microscope (JEOL-JSM-IT 200) connected with an energy-dispersive X-ray spectrometer applying the 20 kV acceleration voltage. HR-TEM JOEL, JAPAN was used to record transmission electron microscope (TEM) images of the nanomaterials and selected area electron diffraction (SAED) pattern. The crystal structures were investigated by the powder X-ray diffraction (XRD) on a POWER-XRD EQUINOX-1000 diffractometer with Cu Kα radiation (λ=1.54056 Å). Furthermore, to determine the chemical states and compositions of catalyst samples, XPS (X-ray photoelectron spectroscopy) with a PHI - VERSAPROBE III spectrometer (micro-focused monochromator with variable spot size) and Fourier transform infrared spectroscopy (FTIR, Perkin Elmer).

Electrode preparation and characterization

All electrochemical measurements were carried out on a Biologic SP-300 Potentiostat electrochemical workstation, the linear sweep voltammograms (LSV) test was carried out in 1 M KOH electrolyte with a scan rate of 10 mV/s three-electrode setup. To prepare catalyst ink, 5.0 mg of the as-prepared ID-CoMo, CoO, MoO electrocatalyst, and 30 µL Nafion (5 wt%) was evenly dispersed in 0.5 mL of propanol, and then the as-obtained solution was treated with ultrasound for 20 min. For comparison, a 0.005 mg/ml commercial IrO_2 and Pt/C suspension was made using a comparable methodology. The as-prepared catalyst ink was smeared onto Ni

foam and dried at 60 ^{o}C for 12 h in a vacuum oven. Before coating, the NF was washed with acetone, HCl aqueous solution, deionized water and ethanol in sequence. In a three-electrode setup nickel foam (NF) as the working electrode, Ag/AgCl (3 M KCl) as reference electrode, and a platinum wire as counter electrode. Measured potentials were referred to the reversible hydrogen electrode (RHE) $\mathbf{E_{(RHE)} = E_{(Hg/HgO)} + 0.923\ V.}$ The resistances of ID-CoMo electrocatalysts were acquired from EIS tests at the overpotential of different mV (vs. RHE) in the frequency scope of 100 kHz to 10 mHz. The durability of RCoFe was tested by cyclic voltammetry (CV) and current-time (i-t) curve tests.

Figure S1. (a, b) FE-SEM images of MoO; (c) Elemental mapping; (d) EDS spectra.

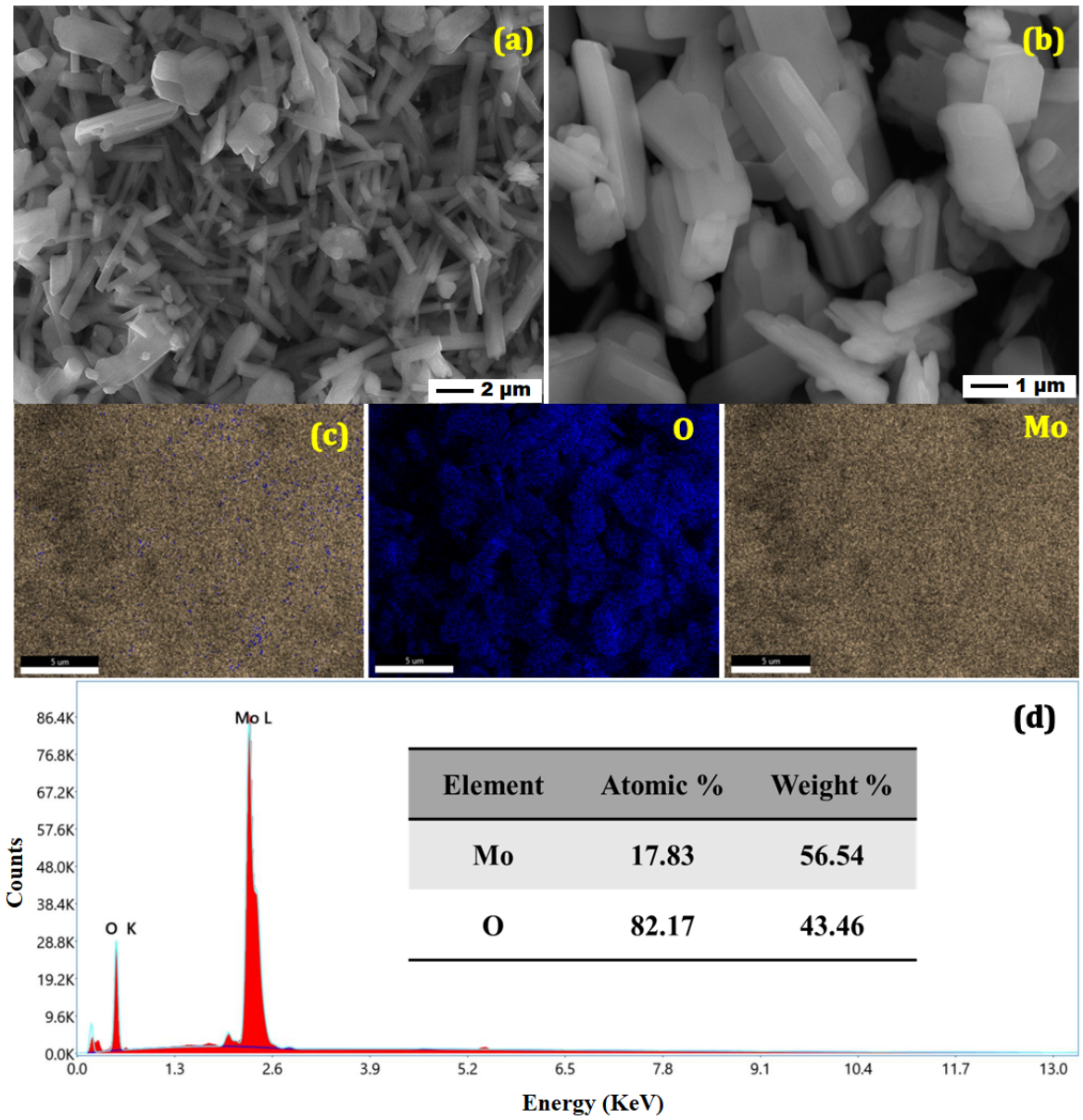

Element	Atomic %	Weight %
Mo	17.83	56.54
O	82.17	43.46

Figure S2. (a, b) FE-SEM images of CoO; (c) Elemental mapping; (d) EDS spectra.

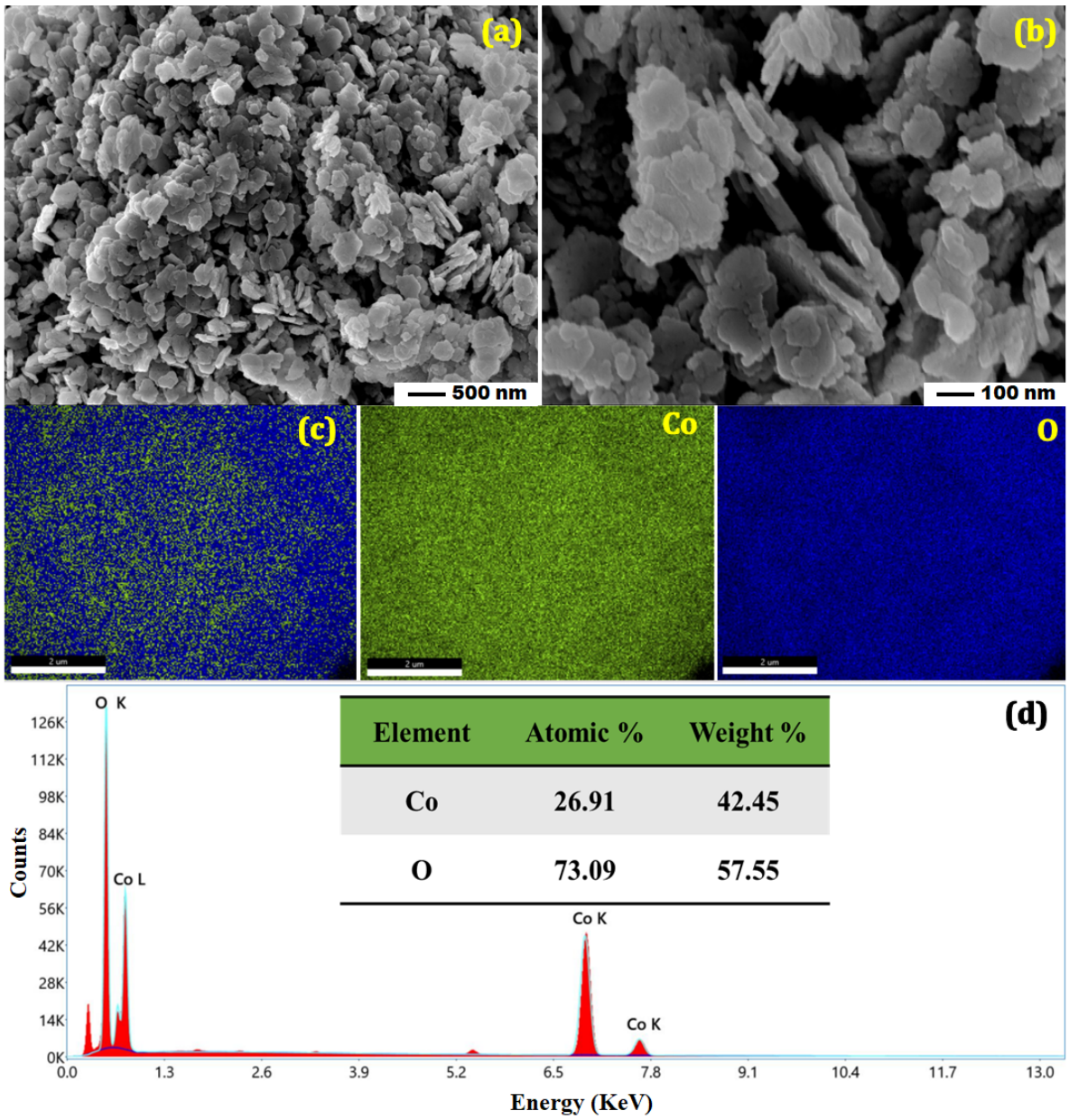

Figure S3: Electrochemical active surface area: (a) ID-CoMo; (b) MoO; (c) CoO and (d) Bare NF

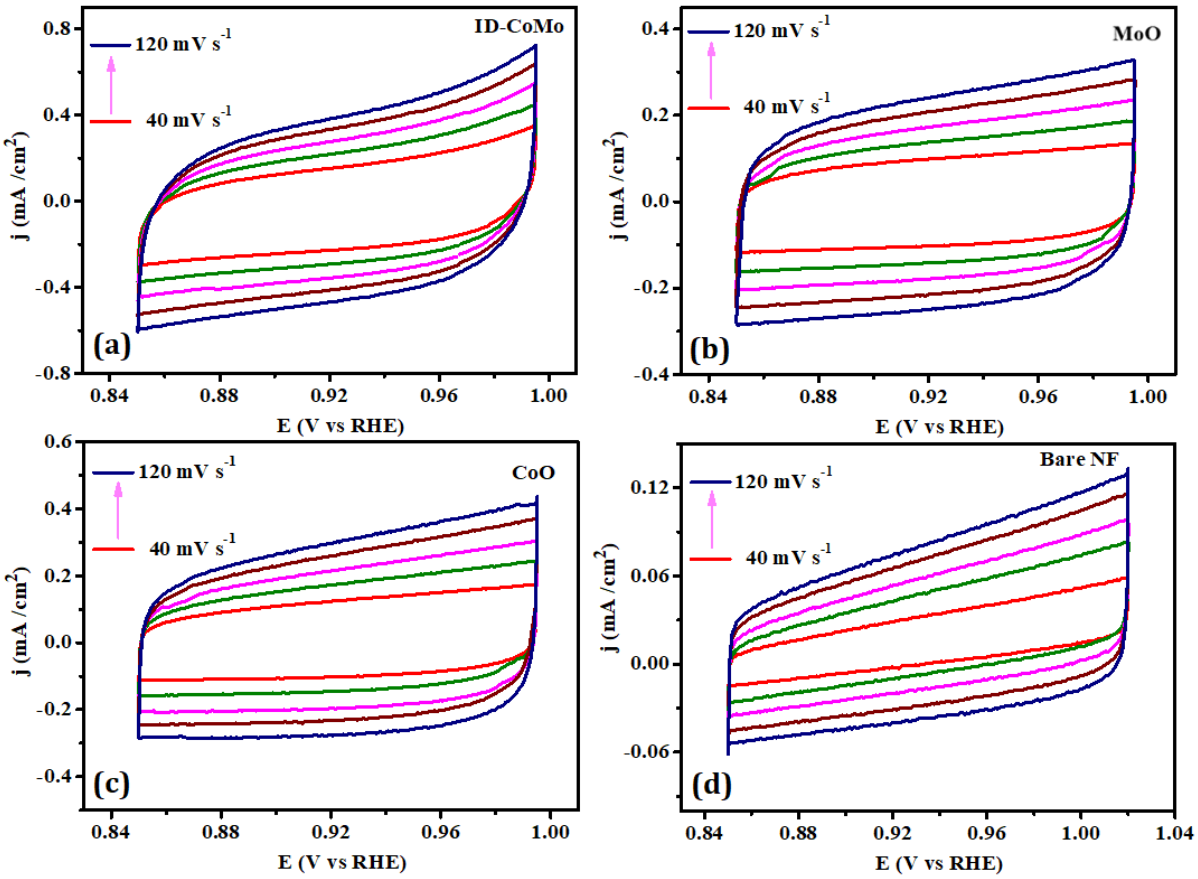

Figure S4: Field emission scanning electron microscope of post OER ID-CoMo: (a, b, c) FE-SEM images in different magnification (inset: Field of view for EM); (d) Elemental mapping (EM); (e) EDS spectra

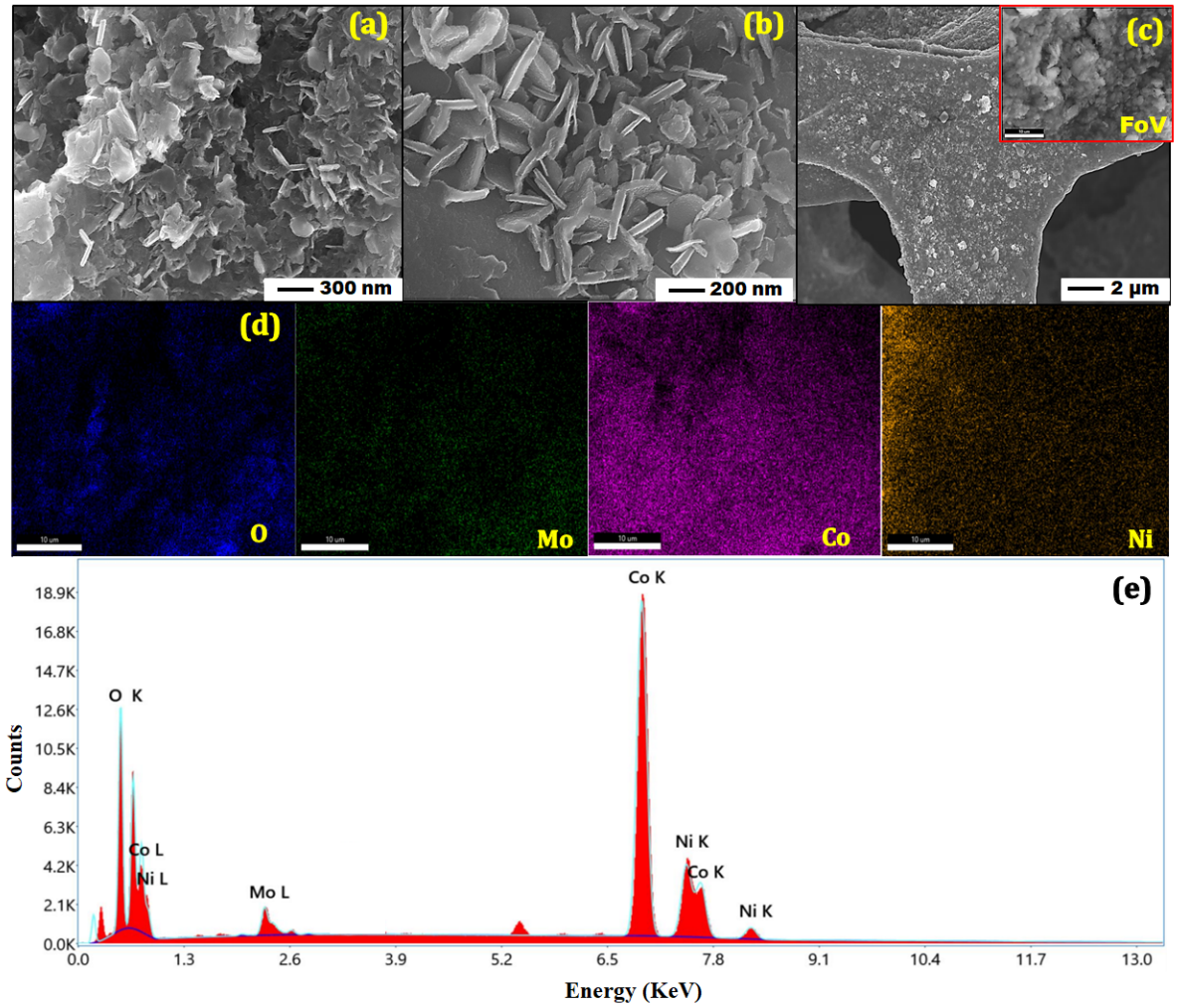

Figure S5: Field emission scanning electron microscope of post HER -ID-CoMo: (a, b, c) FE-SEM images in different magnification (inset: Field of view for EM); (d) Elemental mapping (EM); (e) EDS spectra

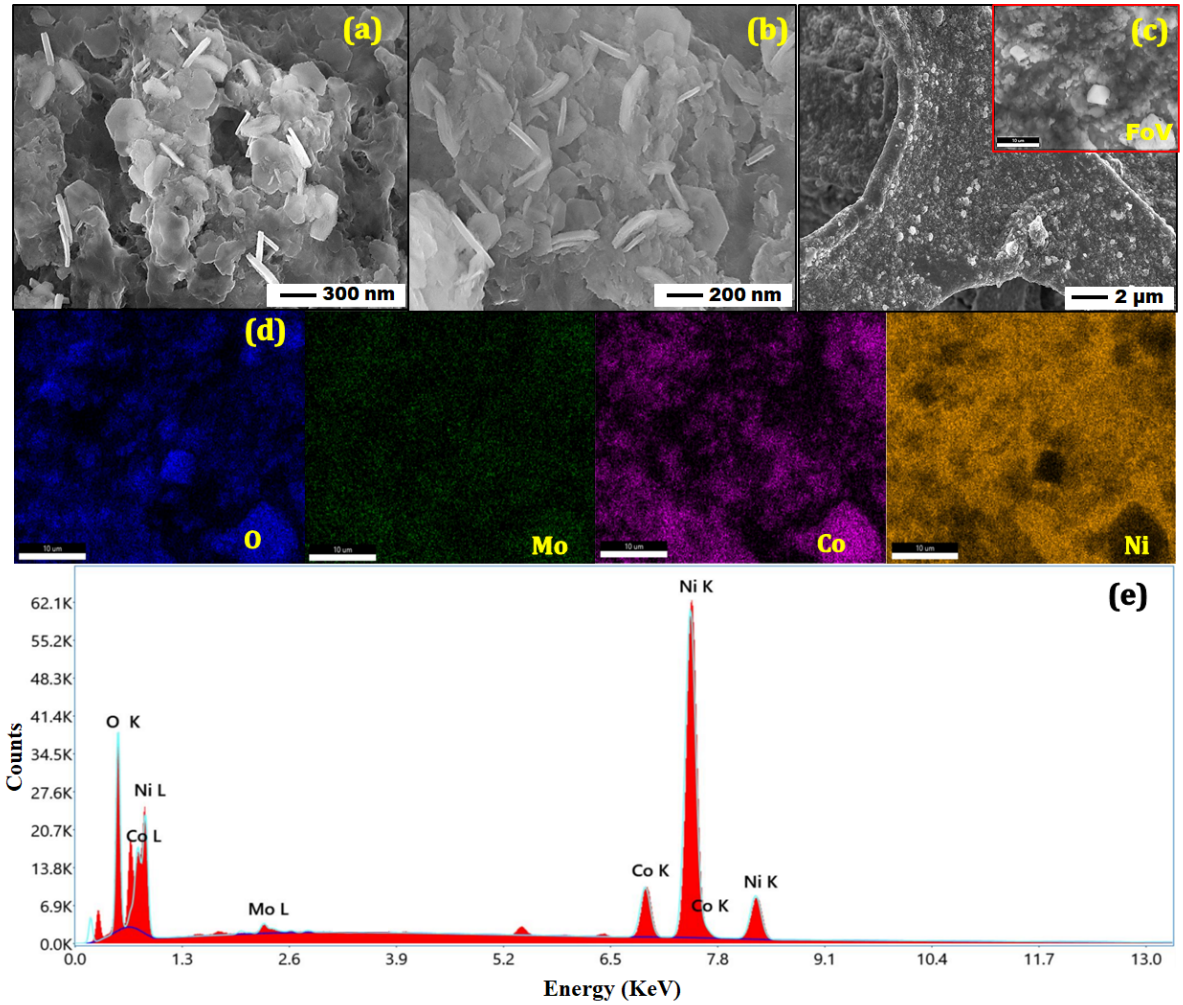

Figure S6: XRD of ID-CoMo after OER and HER.

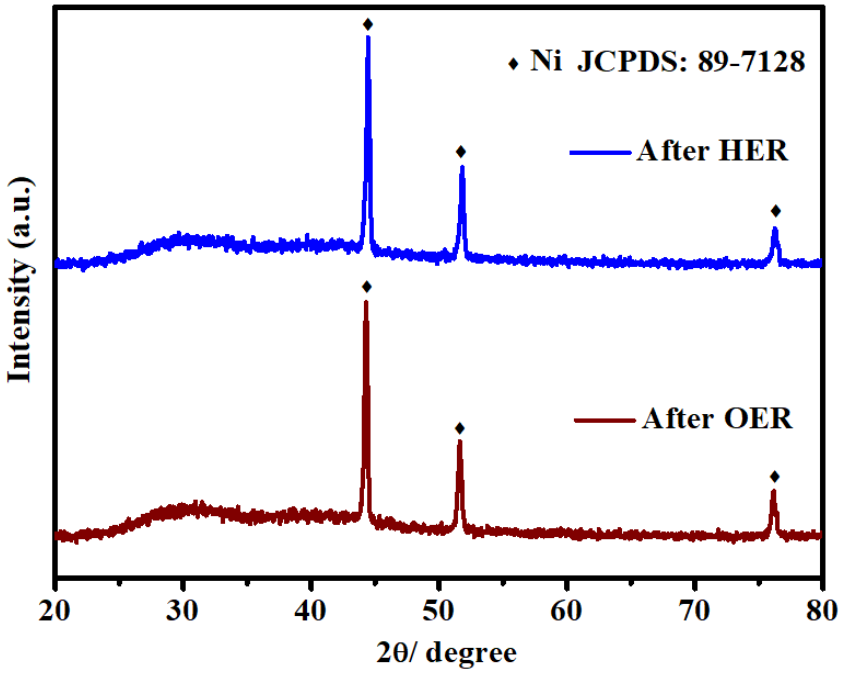

Figure S7: XPS of Mo 3d before and after electrochemical treatment

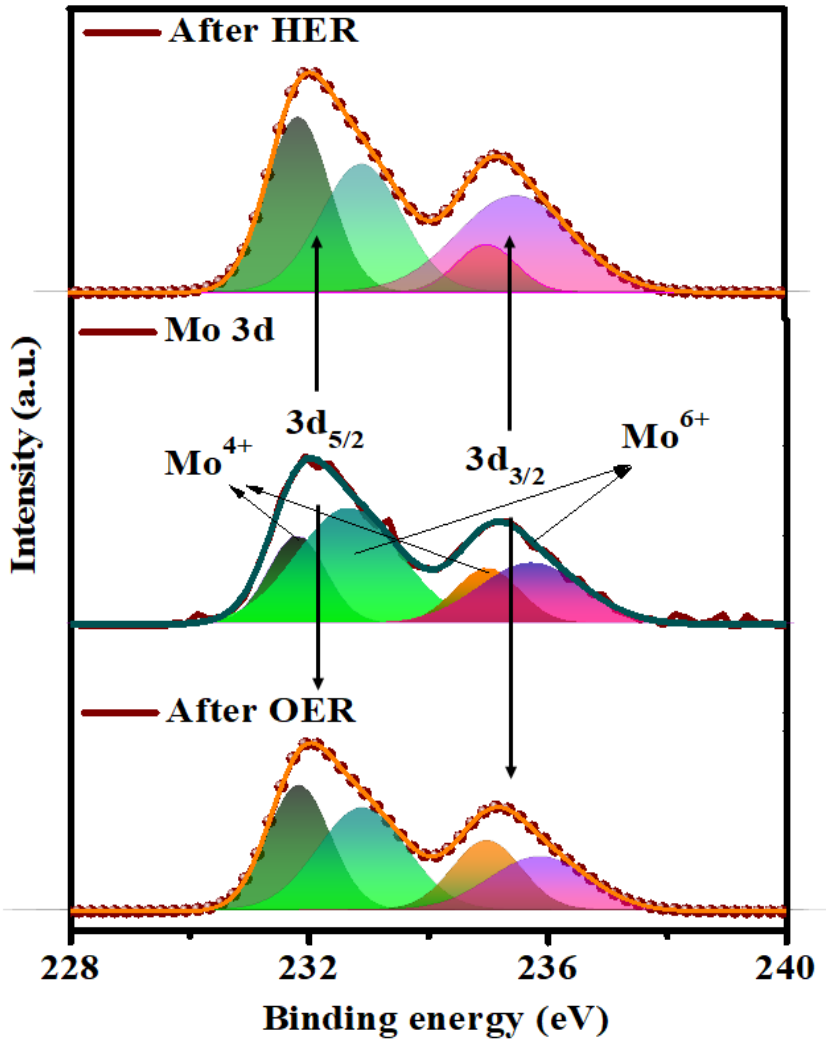

Figure S8: XPS of Co 2p before and after electrochemical treatment

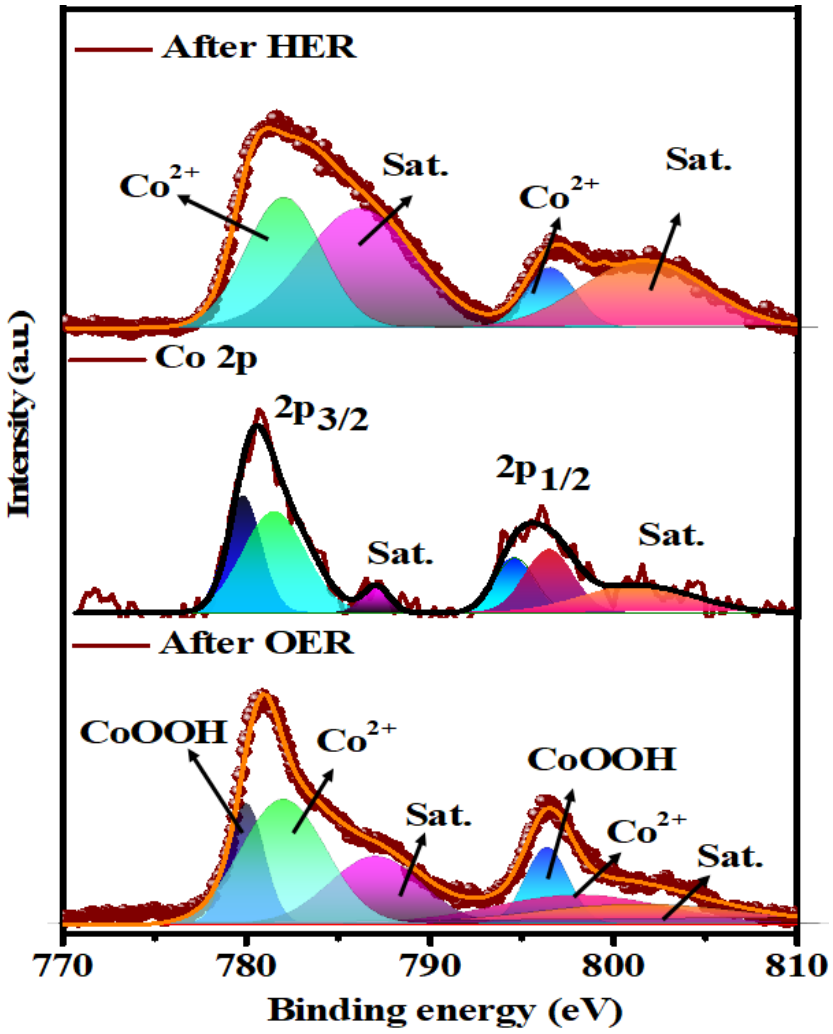

Figure S9: XPS of Co 2p before and after electrochemical treatment

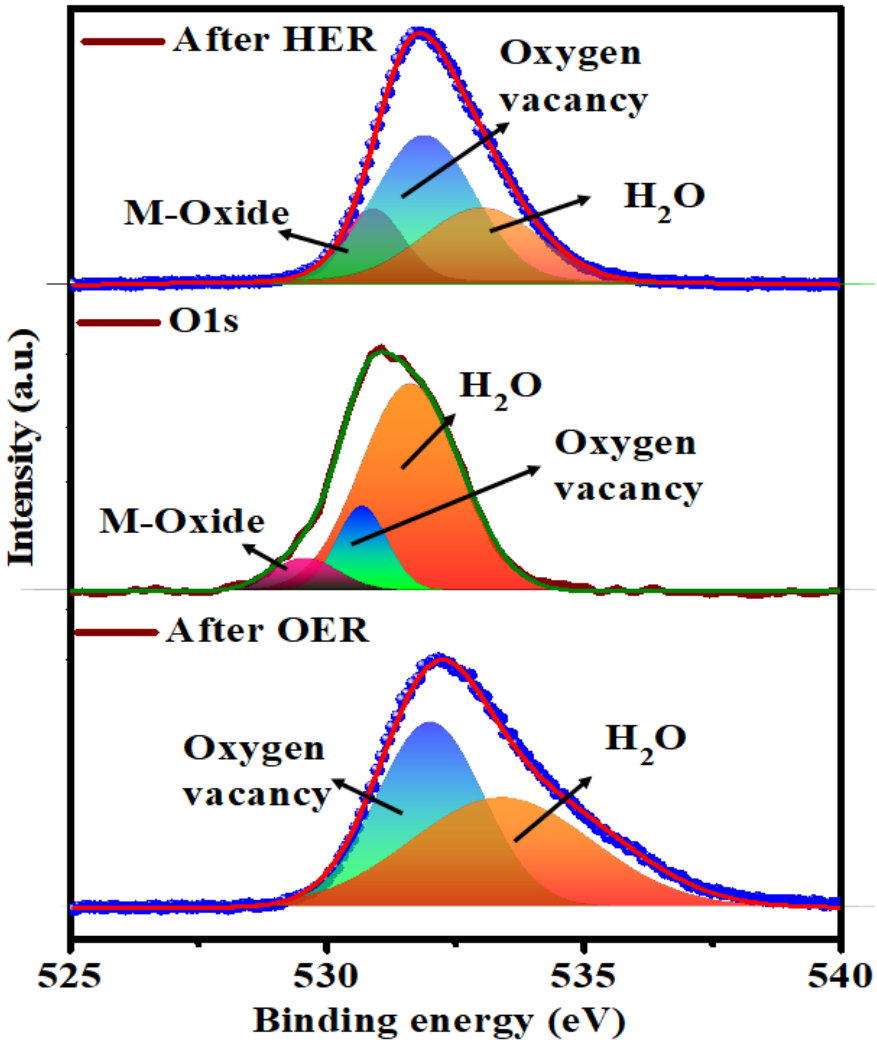

Figure S10: General solar cell water splitting setup

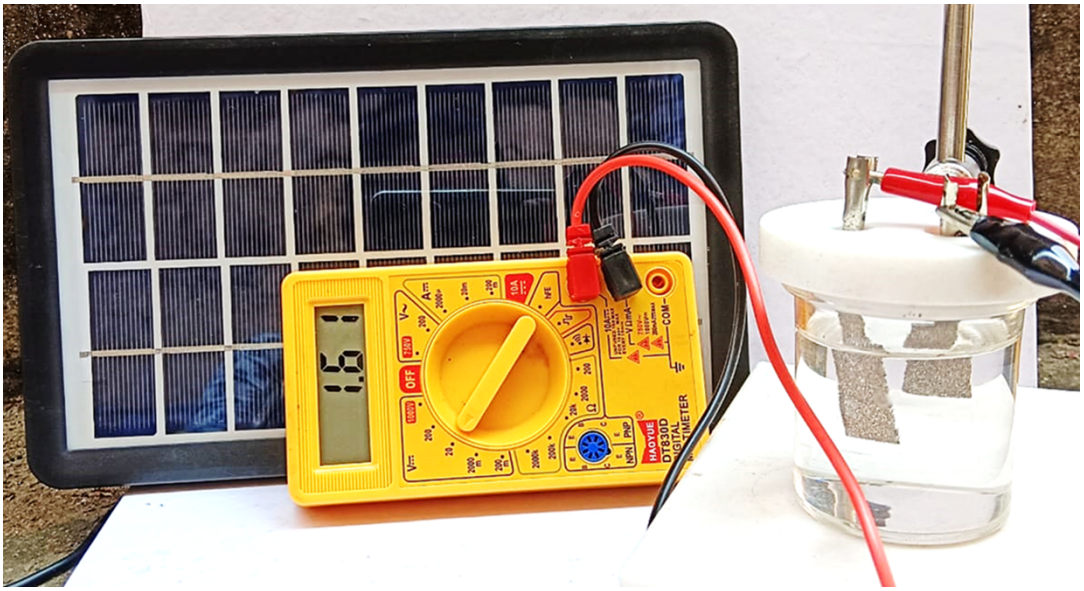

SI-III: Calculations and Tables

SI. C1. RHE Conversion

V (vs. RHE) = $V_{measured}$ (vs. Ag/AgCl) + 0.197 + (0.059 × pH).

SI. C2. Tafel equation

$\eta = a + b \log J$,

where η is the overpotential (V, vs. RHE), b the Tafel slope, and j the corresponding current density (mA /cm^2) as well as the Tafel constant

SI. C3. Turnover frequency (TOF) calculation

The TOF is defined as the number of H_2 or O_2 molecules evolved per site per second

$$\text{TOF of } O_2 \text{ or } H_2 = \frac{J * A}{z * f * n}$$

where, J- Current density (mA/cm^2), A- Geometric surface area of the working electrode, z – no. of electrons involved in the OER and HER process, F- Faraday Constant (96485.3 C mol^{-1}) and n- The number of moles of active sites on the electrode.

SI. C4. ECSA calculation

The capacitive currents are measured in a potential range where no faradic processes occur. The sweep potential is between 0.85 to 1.00 V vs. RHE at different scan rates (40, 60, 80, 100 and 120 mV s^{-1}). The differences in current density variation ($\Delta j = j_a - j_c$) at the potential of 0.925 V vs. RHE plotted against scan rate are fitted to estimate the electrochemical double layer capacitances (C_{dl}), which are used to estimate the electrochemical surface area (ECSA).

$$ECSA = C_{dl} / C_s$$

Where double layer capacitance is C_{dl} and specific capacitance is C_s, and 40 μF cm^{-2} is a constant to convert capacitance to ECSA. The specific capacitance can be converted into an electrochemical active surface area (ECSA) using the specific capacitance value for a flat standard with 1 cm^2 of real surface area.

SI. C5. Faradaic efficiency

Faradaic efficiency of ID-CoMo was calculated by dividing the amount of the experimentally generated gas by the theoretical amount of gas which is calculated by the charge passed through the electrode:

$$\text{Faradic efficiency (\%)} = \frac{(\text{number of moles of gas produced experimentally for a certain time}) * 100}{\text{Theoretically calculated gas production (in mole) for the same time}}$$

The theoretical amount of gas (O_2 and H_2) was calculated from accumulated charge during galvanostatic electrolysis by assuming 100% faradic efficiency. Theoretical amount (n in mole) of gas (H_2, O_2) = Q / (n * F) = (I * t) / (n * F) where Q is the summation of the charge passed through the electrodes, n is the number of electrons which is 2 for HER and 4 for OER and F is the Faraday constant (96485.3 $C.mol^{-1}$).

SI. C6. Calculation of hydrogen generation

Based on the displaced amount of water due to the hydrogen bubbles, the amount of hydrogen generated was calculated using the below relationships.

Amount of hydrogen generated in 1 h = amount of water displaced in litres (1)

$$\text{Amount of hydrogen generated in moles for 1 h} = \frac{\text{Amount of water displaced (litres)}}{\text{22.4 litres}} \quad (2)$$

We also calculated the hydrogen generation rate from the electrical charge passed through the electrode using the equation given below.

$$\left(\begin{array}{c}\text{Current obtained during}\\ \text{water electrolysis}\end{array}\right) \text{X} \left(\begin{array}{c}\text{Time duration for}\\ \text{each potential}\end{array}\right) = \text{Coulomb} \quad (3)$$

$$\frac{\text{Coulomb x F}}{\text{96485 C}} = \text{No. of moles of } e^- \text{ for } H_2 \text{ generation} \quad (4)$$

$$\frac{\text{No. of moles of electron for } H_2 \text{ generation x 1 mole of } H_2 \text{ gas}}{\text{2 moles of electron}} = \text{Moles of Hydrogen generated} \quad (5)$$

Table S1. Recently reported cobalt molybdenum-based catalyst for overall water splitting in 1.0 M KOH

S.No	Catalyst	Electrode	Cell Potential (V)	Reference
1	**ID-CoMo**	**NF**	**1.55**	**This work**
2	CoNiMo-O/H_2 450	NF	1.59	[1]
3	S-CoMoO-12.4	CR	1.61	[2]
4	CMO-1.25	NF	1.63	[3]
5	$Co_6Mo_6C_2$/$Co_2Mo_3O_8$/NP CRGO	CP	1.81	[4]
6	Te-$CoMoO_3$@C	NF	1.54	[5]
7	Co-Mo-P-O	"	1.57	[6]
8	CoP(MoP)-$CoMoO_3$@CN	"	1.55	[7]
9	$MoCo(OH)_2$/CoP/NF	"	1.59	[8]
10	P-CoMoS/CC	CC	1.54	[9]
11	Mo-Co_3O_4/NC	GC	1.62	[10]
12	P–CoMoO4	-	1.48	[11]
13	$Co_xFe_yMo_zO$ NMs	NF	1.68	[12]
14	CoMoP	-	1.56	[13]
15	CoMo@NC-800	CP	1.67	[14]
16	Co-Mo-P/CoNWs	NF	1.495	[15]
17	H-NMO/CMO/ CF-450	CF	1.46	[16]
18	CoMoNx500 NSAs	NF	1.55	[17]
19	Co-Mo-B-P/CF	CF	1.59	[18]
20	NiMo-LDH	GCE	1.62	[19]
21	Mo-CoP_X/NF	NF	1.49	[20]

* CC-Carbon cloth; CF- Copper Foam; CP- Carbon Paper; CR- Carbon Rod; NF-Nickel Foam; GCE- Glassy carbon electrode

Reference.

[1] B. Ren, D. Li, Q. Jin, H. Cui and C. Wang, *ChemElectroChem*, 2019, **6**, 413–420.

[2] J. Dong, S. Chen, C. Lv, M. G. Humphrey, C. Zhang and Z. Huang, *J. Mater. Chem. A*, DOI:10.1039/D3TA07380G.

[3] R. Nadarajan, A. V. Gopinathan, N. P. Dileep, A. S. Sidharthan and M. M. Shaijumon, *Nanoscale*, 2023, **15**, 15219–15229.

[4] R. Liu, M. Anjass, S. Greiner, S. Liu, D. Gao, J. Biskupek, U. Kaiser, G. Zhang and C. Streb, *Chem. Eur. J.*, 2020, **26**, 4157–4164.

[5] L. Wang, H. Yu, S. Zhao, H. Ma, L. Li, F. Hu, L. Li, H. Pan, K. M. El-Khatib and S. Peng, *Inorg. Chem. Front.*, 2022, **9**, 3788–3796.

[6] X. Wang, G. She, L. Mu and W. Shi, *ACS Sustain. Chem. Eng.*, 2020, **8**, 2835–2842.

[7] L. Yu, Y. Xiao, C. Luan, J. Yang, H. Qiao, Y. Wang, X. Zhang, X. Dai, Y. Yang and H. Zhao, *ACS Appl. Mater. Interfaces*, 2019, **11**, 6890–6899.

[8] Y. Xiao, X. Chen, T. Li, Y. Mao, C. Liu, Y. Chen and W. Wang, *Int. J. Hydrogen Energy*, 2022, **47**, 9915–9924.

[9] C. Ray, S. C. Lee, K. V. Sankar, B. Jin, J. Lee, J. H. Park and S. C. Jun, *ACS Appl. Mater. Interfaces*, 2017, **9**, 37739–37749.

[10] X. Zhao, F. Yin, X. He, B. Chen and G. Li, *Int. J. Hydrogen Energy*, 2021, **46**, 20905–20918.

[11] P. Zhou, Z. Li, Y. Zhao, W. Jiang, B. Zhao, X. Chen, J. Wang, R. Yang and C. Zuo, *Int. J. Hydrogen Energy*, 2024, **54**, 1056–1064.

[12] L. Pei, Y. Song, M. Song, P. Liu, H. Wei, B. Xu, J. Guo and J. Liang, *Electrochim. Acta*, 2021, **368**, 137651.

[13] X. Wang, L. Yang, C. Xing, X. Han, R. Du, R. He, P. Guardia, J. Arbiol and A. Cabot, *Nanomaterials*, 2022, **12**, 1098.

[14] R. Ge, J. Huo, Y. Li, T. Liao, J. Zhang, M. Zhu, T. Ahamad, S. Li, H. Liu, L. Feng and W. Li, *J. Alloys Compd.*, 2022, **904**, 164084.

[15] V. H. Hoa, D. T. Tran, D. C. Nguyen, D. H. Kim, N. H. Kim and J. H. Lee, *Adv. Funct. Mater.*, 2020, **30**, 2002533.

[16] Y. Gao, H. Ding, X. Fan, J. Xiao, L. Zhang and G. Xu, *J. Colloid Interface Sci.*, 2023, **648**, 745–754.

[17] Y. Lu, Z. Li, Y. Xu, L. Tang, S. Xu, D. Li, J. Zhu and D. Jiang, *J. Chem. Eng.*, 2021, **411**, 128433.

[18] Y. Wei, P. Zou, Y. Yue, M. Wang, W. Fu, S. Si, L. Wei, X. Zhao, G. Hu and H. L. Xin, *ACS Appl. Mater. Interfaces*, 2021, **13**, 20024–20033.

[19] S. M. N. Jeghan, N. Kim and G. Lee, *Int. J. Hydrogen Energy*, 2021, **46**, 22463–22477.

[20] Y. Yu, J. Li, J. Luo, Z. Kang, C. Jia, Z. Liu, W. Huang, Q. Chen, P. Deng, Y. Shen and X. Tian, *Mater. Today Nano*, 2022, **18**, 100216.